Transfer Learnable Physics-Informed Neural Network Surrogating Grid-Tied Inverters for Renewable Power System Simulation

Canjun Yuan, Changyue Zou, *Senior Member, IEEE*, and Zhicong Huang, *Senior Member, IEEE*

***Abstract*—The development of accurate and reliable dynamic models of grid-tied inverters is essential for system-level simulation and investigation of renewable power system under multi-operating-point (MOP). However, the limited information of commercial inverters caused by privacy issues makes physics-based modeling methods are often ineffective. And existing data-driven approaches lack excellent performance when large transients under extreme disturbances are involved, and cannot provide acceptable out-of-domain generalization performance and unified applicability across diverse scenarios. To address the challenges, this article proposes a novel modeling approach, which is driven by a physics-informed neural network (PINN) embedded with differential algebraic equations (DAEs) structure and the customized loss function. This approach enables the creation of high-precision, physically consistent models for inverters without access to internal information. The obtained models can be further encapsulated as surrogate models, which can be seamlessly integrated into simulation platform as plug-and-play dynamic components, while demonstrating unified applicability across diverse scenarios. Furthermore, cross extrapolation of surrogate models about different inverters is implemented via transfer learning, maintaining accuracy while significantly conserving computational resources and operational data consumption, which is well-suited for inverters with scarce operational data. The effectiveness and superiority of the proposed approach are validated through various case studies, offering promising solutions for the simulation analysis of renewable power system incorporating black-box inverters.**

***Index Terms*—Grid-tied inverters, physics-informed machine learning, simulation-integrated surrogate models, transfer learning**

I. INTRODUCTION

THE rapid growth of renewable energy generation and power electronics technologies is driving the transformation of the legacy power system [1]–[3]. As the crucial power interfaces connecting renewable energy and storage to power grid, grid-tied inverters are widely utilized in renewable power system [4]. In this context, the development of accurate and reliable dynamic models of grid-tied inverters is essential for the design, operation, and analysis of renewable power system [5], [6]. In contrast to direct stability analysis methods using frequency-domain data, time-domain simulation-based methods enable more comprehensive and accurate assessment of dynamic security for renewable power system, providing critical insights to analyse the system's response under multi-operating-point (MOP) and different disturbances [7].

The definitive mathematical models of power electronic converters (PECs) can be established based on physics-based modeling methods when structures and parameters are fully known [8]. However, if the system is too complex, precise derivation could be complicated, leading to a huge computational burden, while excessive simplification and approximation will reduce the applicability of the model. Besides, due to privacy issues, the internal information of commercial inverters is often confidential to system operators or users, rendering physics-based methods nearly ineffective [9]. As another path, data-driven modeling approaches based on measurement data provide more streamlined ideas, eliminating mathematical analysis required by physics-based methods [10].

The feasibility of nonlinear autoregressive models with exogenous inputs (NARX) for time-domain modeling of inverters has been investigated in [11], but the scenarios considered were simple. Meanwhile, recent attempts to apply neural networks (NN) to time-domain modeling of PECs include recurrent neural network (RNN), convolutional neural network (CNN), and long short-term memory neural network (LSTM) [12]–[14]. However, these conventional approaches lack excellent performance in reflecting the transient responses of PECs under extreme disturbances, and they cannot achieve accurate ultra-long-term predictions under arbitrary initial conditions. Besides, the approach proposed in [15] constructs customized models for different modeling scenarios, which does not conform to the original intention of surrogate models that can be used for diverse scenarios. Transformer-based methods achieved improved performance by incorporating attention mechanisms [16], but they are resource intensive and use the generative decoding architecture, which are not well-suited for simulation deployment. On the whole, the above machine learning models are purely data-driven and lack interpretability, which makes them unconvincing in practical applications.

Physics-informed machine learning (PIML) leverages physical knowledge to design network structures and/or loss func-

Manuscript received 26 Mar. 2025, revised 3 Jul. 2025, revised 17 Aug. 2025, accepted 14 Sep. 2025. This work was supported by the National Natural Science Foundation of China under Grant 52577198 and the Guangzhou Municipal Science and Technology Bureau under Grant 2025A04J7064. (Corresponding author: Zhicong Huang)

C. Yuan and Z. Huang are with the Shien-Ming Wu School of Intelligent Engineering, South China University of Technology, Guangzhou, 510006, China (e-mail: zhiconghuang@scut.edu.cn).

C. Zou is with the Electric Power Research Institute, China Southern Power Grid Co., Ltd., Guangzhou, 510663, China. (e-mail: zoucy@csg.cn).

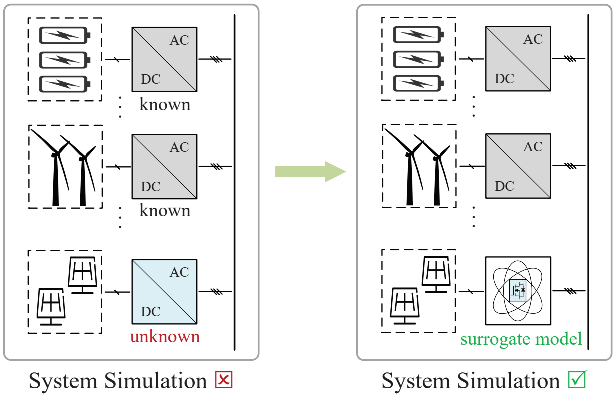

Fig. 1. The surrogate model promotes the simulation of renewable power system incorporating black-box grid-tied inverters.

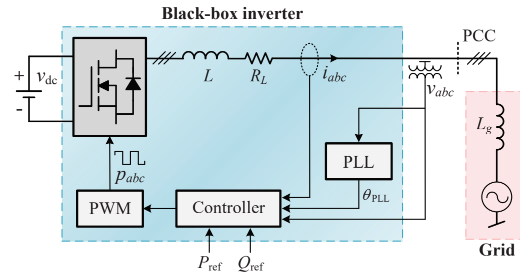

Fig. 2. One-line diagram of the three-phase grid-converter system.

tions, guiding models to obtain explainable and physically consistent solutions [17]–[21]. A physics-in-architecture recurrent neural network for time-domain modeling of dual-active-bridge converter was proposed in [22], but the modeling performance was only verified for steady-state waveforms, and the method requires converter's internal parameters, contradicting the confidentiality of black-box grid-tied inverters.

To address the challenges, this article proposes a novel modeling method, which is driven by a physics-informed neural network (PINN) embedded with differential algebraic equations (DAEs) structure and the customized loss function. This PIML-based approach can provide the high-precision and physically consistent models for grid-tied inverters without access to internal information. In addition, a unified approach is designed to encapsulate NN models of inverters as surrogate models, integrating them as plug-and-play dynamic components into simulation platform to achieve integrated simulation. As illustrated in Fig. 1, the proposed modeling method and model integrating approach make it possible to simulate the renewable power system incorporating black-box inverters.

Normally, the obtained machine learning model can only be used for the specific PEC that is under test, and extensive work needs to be done and huge amount data is required if there are numerous PECs [23], which significantly reduces the modeling efficiency of large-scale renewable power system. This article proposes a transfer learning based cross extrapolation approach for inverter surrogate models, only light effort of re-training is required for source model to be used in other inverters. This approach conserves computational resources and operational data consumption while maintaining accuracy, which is well-suited for inverters with scarce operational data and multi-inverter system.

The main contributions are summarized as follows:

1) The novel PIML-based modeling method for accurate, physics-consistent and partial interpretable black-box inverter modeling with cross-scenario applicability.
2) A unified approach enabling plug-and-play integration of inverter surrogate model in system integrated simulation.
3) Transfer learning reducing data and computation requirements for modeling target inverters through model cross extrapolation.

The rest of this article is organized as follows: Section II provides the systematical explanation of the proposed modeling method. Section III presents the implementation details. Various case studies are provided in Section IV, which validates the effectiveness and superiority of the proposed method, and demonstrates the advantages of cross extrapolation via transfer learning. Finally, Section V concludes this article.

II. Methodology

A. System Description and Problem Definition

Fig. 2 illustrates the one-line diagram of the three-phase grid-converter system, the blue area represents the black-box inverter part under test. Where v_{abc} and i_{abc} denote the voltage and current at the point of common coupling (PCC), v_{dc} denotes the dc-side voltage. System active power instruction P_{ref} and reactive power instruction Q_{ref} determine the operating points of the inverter. L and R_L are the filter inductance and parasitic resistance.

The devices such as phase-locked loop (PLL), pulse width modulation (PWM) and controller exhibit considerable variety, with numerous possible configurations, they introduce nonlinearity and nonideality into the grid-converter system. In this context, the system can be summarized the nonlinear time-varying model as expressed in (1) [24].

$$\begin{aligned} &\frac{d\boldsymbol{x}}{dt} = \boldsymbol{F}_{sys}(\boldsymbol{x}, \boldsymbol{u};\, \lambda,\, t) \\ &\boldsymbol{y} = \boldsymbol{G}_{sys}(\boldsymbol{x}, \boldsymbol{u};\, \lambda,\, t) \\ &\text{s.t. } \boldsymbol{x} \in \mathbb{R}^n,\, \boldsymbol{u} \in \mathbb{R}^r,\, \boldsymbol{y} \in \mathbb{R}^m \end{aligned} \tag{1}$$

where, $\boldsymbol{x}$ is the state vector, $\boldsymbol{u}$ is the external input variables vector, $\boldsymbol{y}$ is the system output variables vector. λ represents the circuit and control parameters, $\boldsymbol{F}_{sys}$ and $\boldsymbol{G}_{sys}$ are the nonlinear operators representing the ordinary differential equations (ODEs) and algebraic equations (AEs) of system. The mapping relationships between system input and output features is implicit, nonlinear and time-varying.

The data-driven time-domain modeling of grid-tied inverter constitutes fundamentally a time-series prediction problem, its goal is to construct a dynamic model with temporal dependence to describe the dynamics of inverter. The dynamic model learns integrated input-output mappings that inherently account for internal phenomena (e.g., modulation, losses, etc.), without requiring explicit topological knowledge. The resulting dynamic model can accurately predicte the temporal trajectory of system output features $\boldsymbol{y}(t)$. As illustrated in

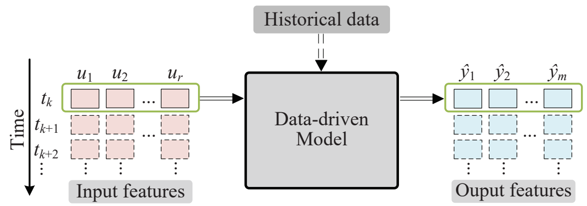

Fig. 3. Stepwise data-driven model based time-domain modeling of grid-tied inverter.

Fig. 3, stepwise data-driven model operates by predicting the current time-step system output $\boldsymbol{y}(t_k)$ through streaming input signals $\boldsymbol{u}(t_k)$ combined with historical system inputs and outputs. This approach aligns with the step-by-step solution mechanism employed in conventional transient simulation.

B. PIML and Transfer Learning Based Modeling Method

Neural ordinary differential equations (NODE) are a widely used method for modeling dynamic system, whose core idea is to use deep neural network (DNN) to parameterize system's ODEs according to universal approximation theorem [25]. Assuming that the system state vector $\boldsymbol{x}(t)$ satisfies the ODEs: $\frac{d\boldsymbol{x}(t)}{dt} = \boldsymbol{f}(\boldsymbol{x}(t))$, the problem of searching for system's ODEs or differential operators in function space is transformed into the problem of optimizing the parameters of DNN [26]:

$$\begin{aligned} &\frac{d\boldsymbol{x}}{dt} = \boldsymbol{F}_{\mathrm{NN}}(\boldsymbol{x};\, \boldsymbol{\theta}) \\ &\boldsymbol{\theta} = \arg\min_{\boldsymbol{\theta}} L(\hat{\boldsymbol{x}}(t),\, \boldsymbol{x}(t)) \\ &\text{s.t. } \hat{\boldsymbol{x}}(t_1) = \boldsymbol{x}(t_1),\, t \in [t_1,\, t_s] \end{aligned} \tag{2}$$

where $\boldsymbol{F}_{\mathrm{NN}}$ is the DNN used to parameterize system's ODEs, $\boldsymbol{\theta}$ denotes its parameters, $L(\cdot)$ is loss function. $\hat{\boldsymbol{x}}(t)$ and $\boldsymbol{x}(t)$ denote the predicted and ground-truth series of state vector, $[t_1,\, t_s]$ is the time interval within which the system evolves.

However, the modeling capability of NODE for system with algebraic constraints is limited [27]. As analyzed in (1), the grid-converter system involves both algebraic constraints and time-varying characteristics, making NODE unsuitable for learning grid-tied inverter behaviors. To address this limitation, this article designs the time-varying differential algebraic neural network (DANN) model based on the DAEs structure, incorporating implicit time variable t. This model comprises two lightweight DNN blocks: $\boldsymbol{F}_{\mathrm{NN}}$ and $\boldsymbol{G}_{\mathrm{NN}}$, which parameterize the ODEs and AEs of the system, respectively.

Some state variables of the black-box grid-tied inverter are unobservable, such as inductor current and capacitor voltage. To address this issue, the DANN model infer the trajectories of state variables using latent states $\boldsymbol{x}$ that circulate exclusively within DANN model. In this context, the entire model can be trained solely using accessible portal data. The general expression of DANN model is as follows:

$$\begin{aligned} &\frac{d\boldsymbol{x}}{dt} = \boldsymbol{F}_{\mathrm{NN}}(\boldsymbol{x},\, \boldsymbol{u},\, \boldsymbol{y};\, \boldsymbol{\theta},\, t) \\ &\boldsymbol{y} = \boldsymbol{G}_{\mathrm{NN}}(\boldsymbol{x},\, \boldsymbol{u};\, \boldsymbol{\zeta},\, t) \\ &\boldsymbol{\theta},\, \boldsymbol{\zeta} = \arg\min_{\boldsymbol{\theta},\, \boldsymbol{\zeta}} L(\hat{\boldsymbol{y}}(t),\, \boldsymbol{y}(t)) \\ &\text{s.t. } \hat{\boldsymbol{y}}(t_1) = \boldsymbol{y}(t_1),\, t \in [t_1,\, t_s] \end{aligned} \tag{3}$$

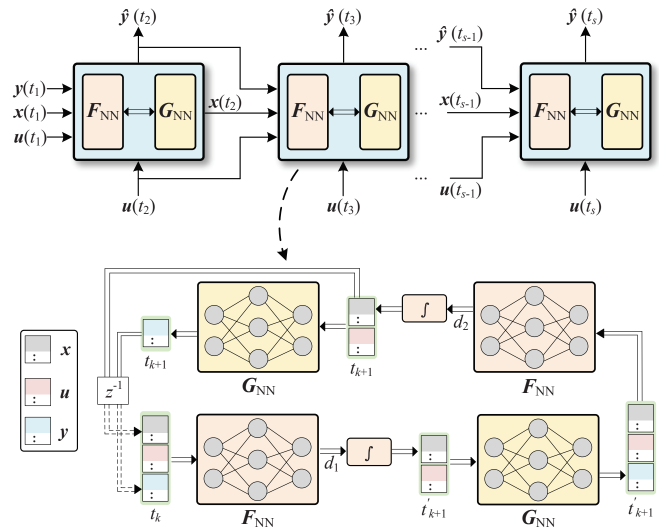

Fig. 4. The unfolded structure of DANN model and its single-step inference process from time t_k to t_{k+1}.

where $\boldsymbol{\theta}$ and $\boldsymbol{\zeta}$ denote model parameters of $\boldsymbol{F}_{\mathrm{NN}}$ and $\boldsymbol{G}_{\mathrm{NN}}$. $\boldsymbol{x}$ is latent states, $\boldsymbol{u}$ is the external input features, $\boldsymbol{y}$ is system output features. $\hat{\boldsymbol{y}}(t)$ and $\boldsymbol{y}(t)$ denote the predicted and ground-truth series of output features, and $\boldsymbol{y}(t_1)$ is the initial value.

By comparing (1) and (3), it can be observed that the DANN model can be regarded as the discretized DAEs of the grid-converter system. It is theoretically feasible to use DANN to parameterize the nonlinear operators $\boldsymbol{F}_{sys}$ and $\boldsymbol{G}_{sys}$ of system and achieve equivalent modeling of the grid-tied inverter.

The unfolded structure and single-step inference process of the DANN model is shown in Fig. 4, where $\boldsymbol{F}_{\mathrm{NN}}$ and $\boldsymbol{G}_{\mathrm{NN}}$ are used twice for inference in each time step, which is determined based on an effective second-order Runge-Kutta numerical integration method. Between the time step t_k and t_{k+1}, the inference formula is as follows, where $t_{k+1} = t_k + \Delta t$, and Δt is the inference time step:

$$\begin{cases} d_1 = \boldsymbol{F}_{\mathrm{NN}}[\hat{\boldsymbol{x}}(t_k),\, \boldsymbol{u}(t_k),\, \hat{\boldsymbol{y}}(t_k);\, \boldsymbol{\theta}] \\ \hat{\boldsymbol{x}}(t'_{k+1}) = \hat{\boldsymbol{x}}(t_k) + d_1 \Delta t \\ \hat{\boldsymbol{y}}(t'_{k+1}) = \boldsymbol{G}_{\mathrm{NN}}[\hat{\boldsymbol{x}}(t'_{k+1}),\, \boldsymbol{u}(t_{k+1});\, \boldsymbol{\zeta}] \end{cases} \tag{4a}$$

$$\begin{cases} d_2 = \boldsymbol{F}_{\mathrm{NN}}[\hat{\boldsymbol{x}}(t'_{k+1}),\, \boldsymbol{u}(t_{k+1}),\, \hat{\boldsymbol{y}}(t'_{k+1});\, \boldsymbol{\theta}] \\ \hat{\boldsymbol{x}}(t_{k+1}) = \hat{\boldsymbol{x}}(t_k) + 0.5(d_1 + d_2)\Delta t \\ \hat{\boldsymbol{y}}(t_{k+1}) = \boldsymbol{G}_{\mathrm{NN}}[\hat{\boldsymbol{x}}(t_{k+1}),\, \boldsymbol{u}(t_{k+1});\, \boldsymbol{\zeta}] \end{cases} \tag{4b}$$

where $\hat{\boldsymbol{x}}(t_{k+1})$ and $\hat{\boldsymbol{y}}(t_{k+1})$ respectively represent the predicted values of latent states $\boldsymbol{x}$ and output features $\boldsymbol{y}$ at time step t_{k+1}, and they will be used for inference in the next time step t_{k+2} as the DANN model is an autoregressive model.

According to Fig. 4, at the beginning of inference, the initial value $\boldsymbol{x}(t_1)$ of latent states is necessary. Therefore, the initial value mapper is established, which calculates initial value $\boldsymbol{x}(t_1)$ based on the accessible initial values $\boldsymbol{u}(t_1)$ and $\boldsymbol{y}(t_1)$:

$$\begin{aligned} &\boldsymbol{x}(t_1) = \boldsymbol{H}_{\mathrm{NN}}(\boldsymbol{u}(t_1),\, \boldsymbol{y}(t_1);\, \boldsymbol{\xi}) \\ &\boldsymbol{\xi} = \arg\min_{\boldsymbol{\xi}} L(\hat{\boldsymbol{y}}(t),\, \boldsymbol{y}(t)) \end{aligned} \tag{5}$$

where $\boldsymbol{H}_{\mathrm{NN}}$ is the DNN denoting the initial value mapper and $\boldsymbol{\xi}$ denotes its parameters.

The raw operational data measured from the system often contain noise, which may adversely affect the accuracy and robustness of the data-driven model. This article employs wavelet transform (WT) for denoising the raw data in the data preprocessing stage. WT is a multi-resolution analysis technique that decomposes signals in both the time and frequency domains, enabling the separation of noise from useful signals:

$$X_w = \int_{-\infty}^{\infty} x(t)\psi_{a,b}(t)\,dt \tag{6}$$

$$\hat{X}_w = \mathrm{sgn}(X_w) \cdot \max(|X_w| - \gamma,\, 0) \tag{7}$$

$$\hat{x}(t) = \frac{1}{C_\psi}\int_{0}^{\infty}\int_{-\infty}^{\infty} \hat{X}_w \psi_{a,b}(t)\,da\,db \tag{8}$$

where, $x(t)$ is the raw data, and $\hat{x}(t)$ is the denoise data. X_w is the wavelet coefficient of signal $x(t)$, and $\hat{X}_w$ is the wavelet coefficient after threshold processing. $\psi_{a,b}(t)$ is the wavelet basis function, a and b represent its scale and translation parameters, and C_ψ is its normalization constant. γ is the noise threshold, typically selected based on the noise level.

Moreover, the measured portal data are not the same scales, so normalization and denormalization are needful to ensure normal model training, the formulas are:

$$y_{\mathrm{nor}} = 2\frac{y_{\mathrm{orig}} - y_{\mathrm{min}}}{y_{\mathrm{max}} - y_{\mathrm{min}}} - 1 \tag{9}$$

$$y_{\mathrm{denor}} = 0.5(y_{\mathrm{nor}} + 1)(y_{\mathrm{max}} - y_{\mathrm{min}}) + y_{\mathrm{min}} \tag{10}$$

where y_{orig} is the original data, y_{max} and y_{min} are the maximum and minimum values in the dataset about feature y, y_{nor} and y_{denor} are the normalized and denormalized result.

To fully utilize physical knowledge, the customized loss function containing physical consistency is design for DANN model based on known physical knowledge of black-box inverters, which includes the data fitting loss component L_{data} and the physical constraint loss component $L_{physics}$:

$$L(\boldsymbol{\theta},\, \boldsymbol{\zeta},\, \boldsymbol{\xi}) = w_{data}L_{data}(\boldsymbol{\theta},\, \boldsymbol{\zeta},\, \boldsymbol{\xi}) + w_{physics}L_{physics}(\boldsymbol{\theta},\, \boldsymbol{\zeta},\, \boldsymbol{\xi}) \tag{11}$$

where w_{data} is the data fitting weight and $w_{physics}$ is the physical constraint weight. Suitable loss weight can balance contributions from data consistency and physical consistency, and make model learns the solution that aligns with both operating data and physical equations.

Assuming that the system has m output features, the batch size of the DANN model is B, and the series length of each feature in single sample is N_s. The loss component L_{data} is defined as (12) when the mean square error (MSE) is selected as the loss form:

$$L_{data} = \frac{1}{m}\sum_{i=1}^{m}\frac{1}{BN_s}\sum_{j=1}^{B}\sum_{k=1}^{N_s}\left(\hat{y}_{i,j}(t_k) - y_{i,j}(t_k)\right)^2 \tag{12}$$

where, $\hat{y}_{i,j}(t_k)$ denotes the predicted value of the ith feature for the jth sample at time t_k, and $y_{i,j}(t_k)$ is the corresponding ground-truth value.

PINN introduces learning biases by incorporating physical equations of the target system into the loss function of machine learning model, guiding the model to converge toward solutions that satisfy physical consistency. The output current dynamics of the commercial black-box grid-tied inverter is the reliably measurable and physically interpretable quantity, which directly reflects the output characteristics of the inverter. At the same time, residual terms of certain voltages in the inverter (e.g., node voltages across the inverter bridge) cannot be obtained due to the unknown internal parameters and structure of the inverter. Therefore, the physical equation satisfied by the inverter output currents (i.e. $i_a + i_b + i_c = 0$) is added to the loss function of the model:

$$L_{physics} = \frac{1}{BN_s}\sum_{j=1}^{B}\sum_{k=1}^{N_s}\left(\hat{i}_{a,j}(t_k) + \hat{i}_{b,j}(t_k) + \hat{i}_{c,j}(t_k)\right)^2 \tag{13}$$

where, $\hat{i}_{a,j}(t_k)$, $\hat{i}_{b,j}(t_k)$ and $\hat{i}_{c,j}(t_k)$ are the predicted values of the grid-side currents for the jth sample at time t_k. The DANN model with $L_{physics}$ can learn the physical invariants existing in the system based on unsupervised learning strategies.

Algorithm 1 Modeling Process of the Proposed Method.

Input: Features $\boldsymbol{u}^{r\times s\times q}$ and $\boldsymbol{y}^{m\times s\times q}$ measured under q operating points, training epoch M, learning rate α, loss threshold e_{min}, hyperparameters of PIML-based model.
Output: The PIML-based model of the inverter under test.

Collecting measurement data $\boldsymbol{u}^{r\times s\times q}$ and $\boldsymbol{y}^{m\times s\times q}$, data denoising and normalize them to dataset $(\boldsymbol{U},\, \boldsymbol{Y})$.
Splitting the dataset $(\boldsymbol{U},\, \boldsymbol{Y})$ into training set $(\boldsymbol{U}_{\mathrm{train}},\, \boldsymbol{Y}_{\mathrm{train}})$, validation set $(\boldsymbol{U}_{\mathrm{val}},\, \boldsymbol{Y}_{\mathrm{val}})$ and test set $(\boldsymbol{U}_{\mathrm{test}},\, \boldsymbol{Y}_{\mathrm{test}})$.
Initializing model.
for $i = 1$ to M **do**
  Calculating predicted features series $\hat{\boldsymbol{y}}(t)$.
  Calculating loss L based on (11).
  if $L < e_{\mathrm{min}}$ **then**
    Stop training and save model.
  else
    Calculating the gradient of loss $\frac{\partial L}{\partial \boldsymbol{\theta}}$, $\frac{\partial L}{\partial \boldsymbol{\zeta}}$ and $\frac{\partial L}{\partial \boldsymbol{\xi}}$.
    Updating model using gradient and learning rate.
    Updating learning rate α.
  end if
  Verifying the generalization ability of PIML-based model using validation set $(\boldsymbol{U}_{\mathrm{val}},\, \boldsymbol{Y}_{\mathrm{val}})$.
end for
Saving PIML-based model.
Testing the modeling performance of PIML-based model using test set $(\boldsymbol{U}_{\mathrm{test}},\, \boldsymbol{Y}_{\mathrm{test}})$.

The proposed PIML-based modeling method includes two key points. The PINN embedded with DAEs structure introduces inductive biases, and the loss function containing physical consistency introduces learning biases. The inductive biases and learning biases based on physical knowledge enable the modeling method to better learn temporal dependencies and explore the underlying physical properties of the grid-tied inverter. The modeling process is illustrated in Algorithm 1.

Training individual model for each grid-tied inverter in the large-scale renewable power system lead to significant computational resource consumption, and training from scratch may fails to achieve the accurate model for inverters with scarce

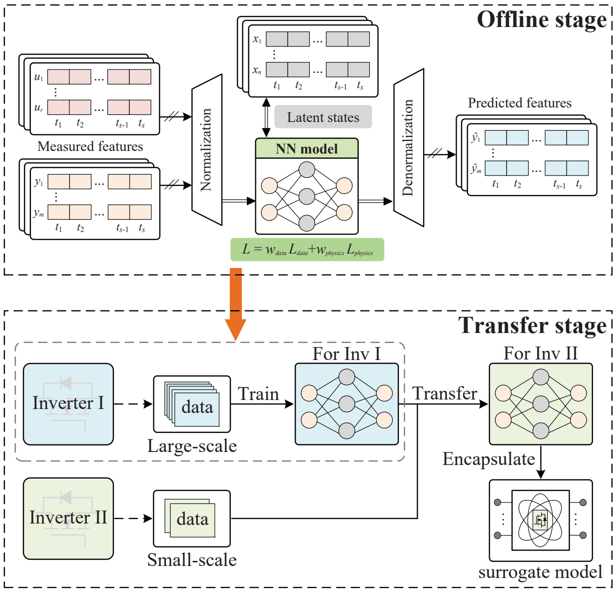

Fig. 5. Framework of the proposed modeling method based on PIML and transfer learning.

operational data. To address this challenge, we propose leveraging transfer learning to fine-tune existing pre-trained models, thereby achieving cross extrapolate of surrogate models about different inverters.

Based on the existing model of source inverter I and small-scale operational data of target inverter II, the surrogate model of target inverter can be quickly obtained. This approach enables the reuse of knowledge (encoding DAEs parameters and feature extraction layers) learned from source inverter and facilitates quick adaptation to target inverter, thus reducing operational data consumption, which is well-suited for inverters with scarce operational data. The framework of the proposed modeling method based on PIML and transfer learning is shown in Fig. 5.

III. Model Training and Surrogating in Simulation

A. System Settings and Data Acquisition

A three-phase grid-tied inverter detailed model that incorporates dynamic and non-linear characteristics (e.g., controller saturation) is constructed to obtain training data as close as possible to real-world conditions for the proposed modeling method, whose topology structure shown in Fig. 2 and system parameters are shown in Table I. The hardware platform is a workstation with Intel i9-12900K CPU, 64GB RAM, and NVIDIA 3090ti GPU. The external inputs $\boldsymbol{u}$ contain v_{dc}, v_{abc}, P_{ref} and Q_{ref}, the output features $\boldsymbol{y}$ contain i_{abc}, other electrical quantities are considered as latent states $\boldsymbol{x}$ due to unobservability.

Set different external inputs to operate the grid-tied inverter at different operating points (P_{ref}: 5 to 15 kW, Q_{ref}: -3 to 3 kvar). Set the sampling rate to 10 kHz and acquire 500 sets of operational data at different operating points, divide 20% of these operational data into training set, 40% into validation set, and 40% into test set.

TABLE I
Parameters of Grid-Tied Inverter

Parameter description	Value
DC voltage v_{dc}	800 V
Grid line-voltage v_{grid}	400 V
Grid frequency f_0	50 Hz
Switching frequency f_{sw}	10 kHz
Filter inductor L	8 mH
Parasitic resistance of filter inductor R_L	0.08 Ω
Proportional parameter of the current controller K_{p_i}	5
Integral parameter of the current controller K_{i_i}	10
Proportional parameter of the PLL K_{p_PLL}	10
Integral parameter of the PLL K_{i_PLL}	5000

B. Samples Generation and Training Results

As noted in reference [28], the stiffness problem in dynamic system modeling can be addressed by dividing long-time trajectories of the training dataset into multiple short segments for model learning. Considering grid-tied inverter as typical stiff system, the training samples generation method in this article is to randomly extract B data segments with arbitrary starting point of length l from the operational curves during each training epoch, which as B single training sample in each mini-batch. Based on this samples generation method, the trained PIML-based model of inverter can start predicting from arbitrary initial values without being limited to the initial values of training set.

The training samples length l is a key hyperparamete for balancing between accuracy and stiffness of the PIML-based model [28]. The model performance under different training samples length is shown in Fig. 6(a), the final selected training samples length is 110. The suitable weights of the loss function in (11) can balance the contributions of data consistency and physical consistency, thereby ensuring solution that satisfy both operating data and physical equations while enhancing the model's generalization capability. The model performance under different loss weights is shown in Fig. 6(b), the final selected data fitting weight w_{data} is 1.0 and physical constraint weight $w_{physics}$ is 0.5. Other relevant hyperparameters after trial-and-error are shown in Table II.

TABLE II
Hyperparameters Setting of the PIML-based Model

Hyperparameters	Value	Hyperparameters	Value
H_{NN} layer neurons	16	Optimizer	Adam
F_{NN} layer neurons	64, 64	Loss function	MSE
G_{NN} layer neurons	16	Initial learning rate	0.05
Latent states number	4	Decay factor	0.95
Training samples length	110	Batch size	128
Data fitting weight	1.0	Physical constraint weight	0.5

The model is trained for 10000 epochs with a validation frequency of 500 epochs, and learning rate decay exponentially every 100 epochs. The training process lasted for 55 minutes, and the loss convergence process is shown in Fig. 7. Final loss on both training and validation sets is lower than 2×10^{-6}, indicating that the learned model has considerable accuracy and generalization ability.

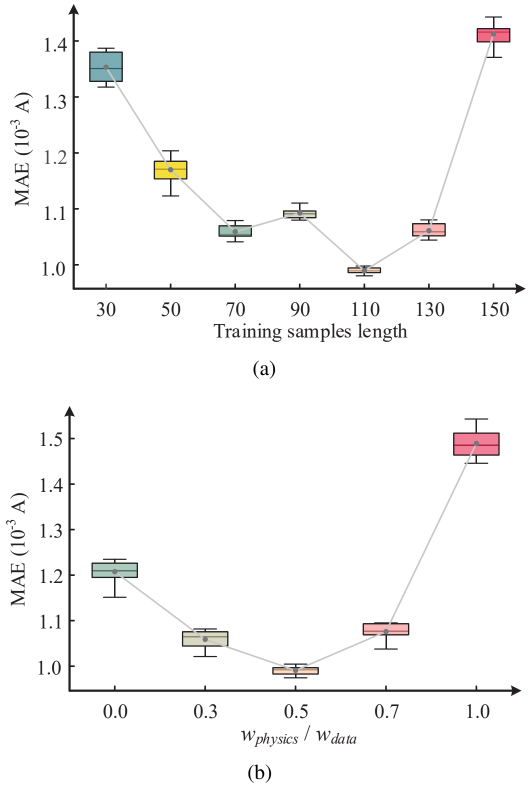

Fig. 6. Sensitivity analysis of key hyperparameters' impact on modeling performance (test samples length is 2000 for evaluating ultra-long-term prediction performance). (a) Length of training samples. (b) Ratio of physical constraint weight.

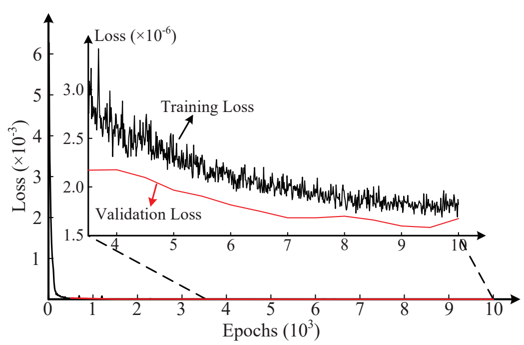

Fig. 7. Loss convergence process on training and validation sets.

To highlight the superiority of the proposed method, representative data-driven models (RNN and LSTM) and physics-informed approach (NODE) [21] are employed as benchmarks. As shown in Table III, which presents the error metrics of different algorithms on validation set, this article proposed method achieves superior performance across all evaluation metrics.

C. PIML-based Models Surrogating Into Simulation

The dominant paradigm for circuit system-level simulation is combining models of individual components, then the entire

TABLE III
ERRORS OF DIFFERENT ALGORITHMS ON VALIDATION SET

Algorithm	MSE (10^{-6})	RMSE (10^{-3})	MAE (10^{-3})	MAPE
RNN	11.263	3.355	2.037	10.33%
LSTM	2.330	1.526	1.145	4.48%
NODE	2.740	1.655	1.274	7.23%
This article	**1.636**	**1.279**	**0.992**	**4.41%**

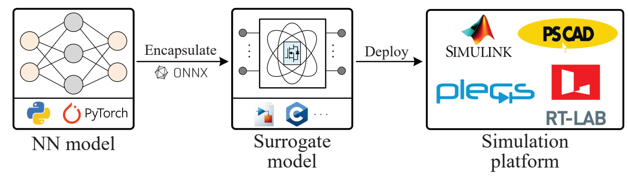

Fig. 8. The encapsulation and deployment process of the surrogate model for grid-tied inverter.

system can be mathematically represented using ODEs:

$$\frac{d\boldsymbol{x}}{dt} = f(\boldsymbol{x}, \boldsymbol{u}; \mu, t) \quad \text{s.t. } \boldsymbol{x}(T_0) = \boldsymbol{x}_0, \; t \in [T_0, T_1] \tag{14}$$

where, $\boldsymbol{x}$ denotes the system states, $\boldsymbol{u}$ denotes the external inputs, μ represents system parameters. f governs the state evolution on the discrete time mesh $[T_0, T_1]$ and $\boldsymbol{x}_0$ denotes the initial value of system states.

The approximate time trajectory $\boldsymbol{x}(t)$ of system states can be calculated step-by-step by solving these ODEs on time mesh $[T_0, T_1]$ based on numerical solvers (e.g., *Runge-Kutta*), which is defined as the initial value problems (IVP):

$$\boldsymbol{x}(t) \approx ODESolver(\boldsymbol{x}_0, \Delta t, T_0, T_1, \mu) \tag{15}$$

where, T_0 and T_1 are the starting and ending of the time mesh, Δt is the simulation step. According to (4), (15) and Fig. 3, the PIML-based model calculates the trajectory of system features $\boldsymbol{y}(t)$ step-by-step, this stepwise inference mechanism is in line with the solving mechanism of simulation.

Based on the feasibility analysis above, a unified approach is designed to encapsulate NN models of inverters as surrogate models that can be used as plug-and-play dynamic components for integrated simulation. As shown in Fig. 8, the PIML-based NN model of inverter is converted into an independent numerical file (e.g., *.onnx*), which is then encapsulated as the surrogate model (e.g., *.slx*) with input-output ports. The surrogate models with arbitrarily configurable initial values can seamlessly integrate into simulation platform, which are consistent with actual inverter equipments. As illustrated in Fig. 1, the proposed modeling method and model integrating approach make it possible to simulate the renewable power system incorporating black-box inverters.

IV. CASE STUDY AND VALIDATION

Various case studies are designed to validate the proposed modeling method. The obtained PIML-based surrogate model of grid-tied inverter is integrated into Simulink platform according to the approach shown in Fig. 8, and verify actual simulation performance of surrogate model in diverse scenarios.

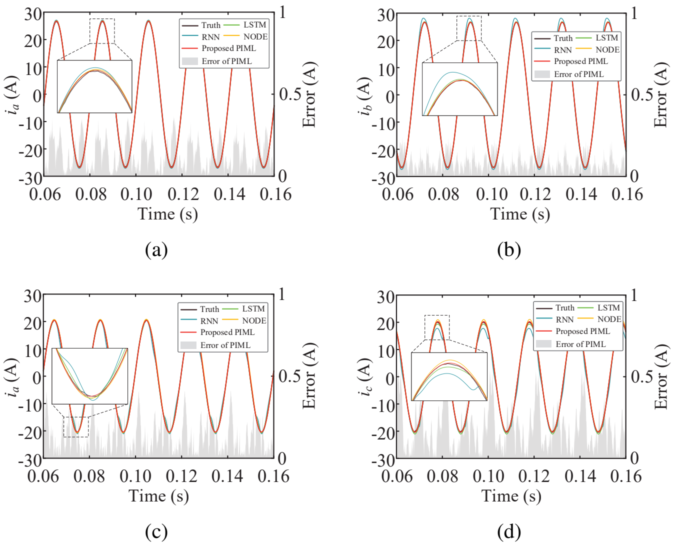

Fig. 9. Measurement and estimation of partial output features. (a)-(b) Experiment A-1: steady state waveforms. (c)-(d) Experiment A-2: small disturbance of dc-side voltage.

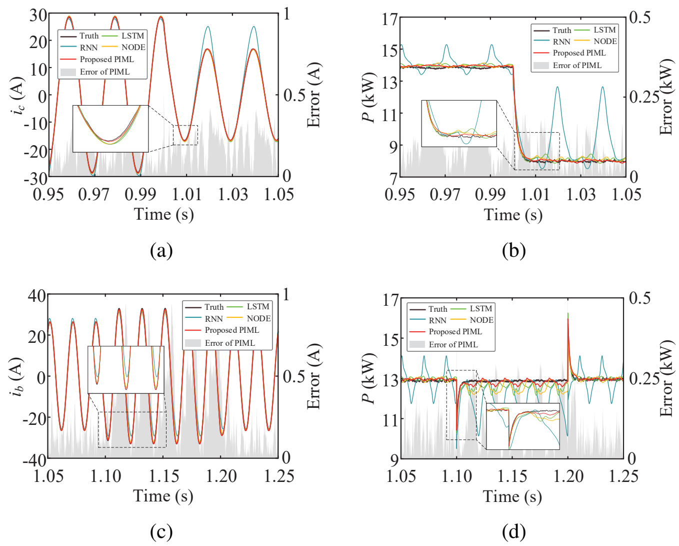

Fig. 10. Measurement and estimation of partial output features. (a)-(b) Experiment B-1: power instructions change. (c)-(d) Experiment B-2: short circuit fault.

Notably, unlike previous studies, the PIML-based surrogate model can be applied to diverse scenarios without the need to build customized models for different scenarios, which conforms to the original intention of surrogate models. Representative data-driven models (RNN and LSTM) and physics-informed approach (NODE) [21] are used as benchmarks to highlight the superiority of the proposed modeling method.

To fairly compare with other methods, the accuracy of surrogate models is evaluated by mean absolute error (MAE) and coefficient of determination (R^2), their formulas are shown:

$$\mathrm{MAE} = \frac{1}{N}\sum_{i=1}^{N}|y_i - \hat{y}_i| \tag{16}$$

$$R^2 = 1 - \frac{\sum_{i=1}^{N}(y_i - \hat{y}_i)^2}{\sum_{i=1}^{N}(y_i - \bar{y})^2} \tag{17}$$

where N is the number of the observation points, y_i and $\hat{y}_i$ are the ground-truth and predicted values of observation points, and $\bar{y}$ is the mean of the ground-truth values. Lower MAE values and R^2 closer to 1 indicate higher model accuracy, while consistently high accuracy metrics across different modeling scenarios demonstrate the model's superior performance.

A. Steady State and Small-signal Modeling Scenarios

1) Experiment A-1: Steady State Waveforms:

When setting P_{ref} to 13 kW and Q_{ref} to 2 kvar, partial steady state waveforms are shown in Fig. 9 and the complete accuracy metrics for different features are shown in Table IV. The LSTM, NODE and PIML-based model have higher accuracy, while the RNN model has slight errors.

2) Experiment A-2: Voltage Disturbance of DC-Side:

Set P_{ref} to 10 kW and Q_{ref} to -1 kvar. The partial estimation results of grid-side current are depicted in Fig. 9 when dc-side voltage with a sine disturbance of 20 V and 100 Hz, the detailed accuracy metrics are in Table IV.

The current waveforms predicted by RNN model show significant distortion, and the prediction of LSTM and NODE model show slight differences compared to actual waveforms. In contrast, the PIML-based surrogate model accurately mirrors current responses under small-signal disturbances.

B. Large-signal Modeling Scenarios

1) Experiment B-1: Power Instructions Change:

In actual operation of grid-tied inverters, power instructions will be adjusted according to actual conditions, the effectiveness of surrogate models under MOP is necessary.

Set Q_{ref} to 2 kvar and reduce P_{ref} from 14 kW to 8 kW at 1 s, the estimation results and accuracy metrics are shown in Fig. 10 and Table V. The RNN model becomes unstable after P_{ref} changes (i.e. operating point changes), and the PIML-based model shows better performance than LSTM and NODE model.

2) Experiment B-2: Short Circuit Fault:

The effectiveness of surrogate models in reflecting transients process of grid-tied inverters under extreme disturbances is necessary.

Set P_{ref} to 13 kW and Q_{ref} to 1 kvar, and three-phase short circuit fault is set on grid at 1.1 s, causing the grid voltage to drop to 80% of steady state value, and the fault to be cut off after 0.1 s. The presence of short circuit fault leads to a increase in current in a short period of time. The estimation results and accuracy metrics are shown in Fig. 10 and Table V. The PIML-based model's results are essentially in line with the truth operating data curves, whereas the RNN, LSTM and NODE model's prediction is less satisfactory and does not fit the truth curves better in the crest and trough parts.

C. Out-of-Domain Generalization Performance

In addition to having excellent in-domain generalization ability, surrogate models are also expected to have reliable

TABLE IV
ACCURACY METRICS OF EXPERIMENT A-1 AND A-2

Features	Metrics	Experiment A-1				Experiment A-2			
		RNN	LSTM	NODE	PIML	RNN	LSTM	NODE	PIML
i_a (A)	MAE	0.427	0.147	0.189	**0.130**	0.670	0.290	0.449	**0.125**
	R^2	0.9993	0.9999	0.9998	**0.9999**	0.9952	0.9994	0.9984	**0.9999**
i_b (A)	MAE	0.763	0.155	0.112	**0.081**	1.133	0.402	0.266	**0.140**
	R^2	0.9970	0.9999	0.9999	**0.9999**	0.9904	0.9985	0.9995	**0.9999**
i_c (A)	MAE	0.690	0.203	0.175	**0.110**	1.213	0.390	0.475	**0.178**
	R^2	0.9978	0.9998	0.9998	**0.9999**	0.9891	0.9989	0.9985	**0.9998**
P (W)	MAE	472.9	108.4	105.5	**72.6**	562.6	246.2	155.1	**77.8**
Q (var)	MAE	88.3	49.8	48.5	**29.9**	419.7	94.3	157.0	**70.2**

TABLE V
ACCURACY METRICS OF EXPERIMENT B-1 AND B-2

Features	Metrics	Experiment B-1				Experiment B-2			
		RNN	LSTM	NODE	PIML	RNN	LSTM	NODE	PIML
i_a (A)	MAE	0.574	0.214	0.307	**0.170**	0.957	0.433	0.544	**0.310**
	R^2	0.9977	0.9997	0.9995	**0.9998**	0.9956	0.9992	0.9988	**0.9996**
i_b (A)	MAE	1.434	0.189	0.248	**0.109**	1.400	0.376	0.477	**0.259**
	R^2	0.9787	0.9998	0.9996	**0.9999**	0.9906	0.9993	0.9992	**0.9997**
i_c (A)	MAE	1.267	0.263	0.234	**0.175**	1.299	0.241	0.423	**0.156**
	R^2	0.9807	0.9997	0.9997	**0.9999**	0.9900	0.9998	0.9993	**0.9999**
P (W)	MAE	742.6	141.8	129.9	**85.9**	776.4	192.9	216.2	**97.3**
Q (var)	MAE	286.4	72.2	125.8	**62.6**	149.2	92.7	**83.6**	106.3

out-of-domain generalization performance.

1) Experiment C-1: Extrapolation of Initial Conditions:

The dataset acquired in Section III-A does not include the initial conditions for transitioning from no-load to steady-state.

Set P_{ref} to 10 kW and Q_{ref} to -1.5 kvar, the estimation results and accuracy metrics are shown in Fig. 11 and Table VI. The RNN model cannot generalize the transient process well and show obvious fluctuation. LSTM and NODE model has certain errors at the initial time, while PIML-based model provides accurate predictions based on the full utilization of physical knowledge.

2) Experiment C-2: Extrapolation of Operating Points:

The operating points (i.e. power instructions) range acquired in Section III-A is limited, the surrogate models that are valid out-of-domain will help with the wide operating conditions simulation of renewable power system.

Set P_{ref} to 17 kW and Q_{ref} to 1 kvar, the estimation results and accuracy metrics are shown in Fig. 11 and Table VI. Similar to experiment C-1, the PIML-based model still has the best modeling performance.

In a nutshell, the above cases verify that the PIML-based surrogate model can provide accurate, physically consistent, and reliable modeling performance, whether in steady state, small-signal conditions, large-signal conditions and out-of-domain extrapolation.

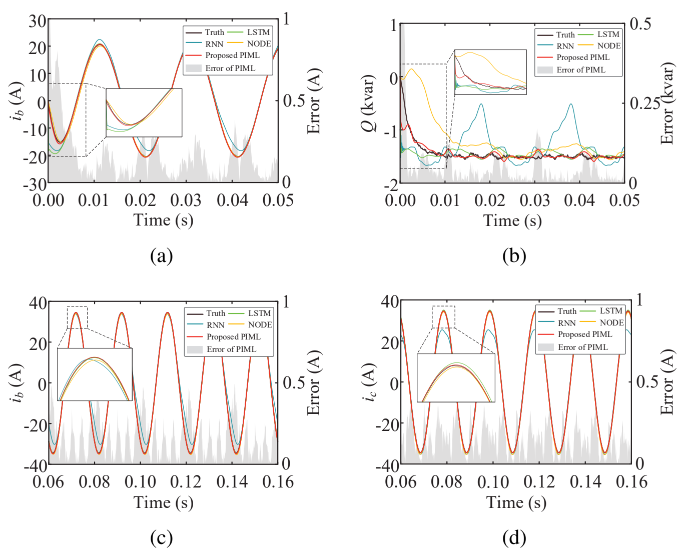

Fig. 11. Measurement and estimation of partial output features. (a)-(b) Experiment C-1: extrapolation of initial conditions. (c)-(d) Experiment C-2: extrapolation of operating points.

D. Transfer Learning Based Cross Extrapolation of Surrogate Models

Construct the multi-inverter system as shown in Fig. 12 to investigate the advantages of proposed modeling method with transfer learning in improving modeling efficiency and operational data consumption. The parameters of inverter A are the same as those in III-A, and the parameters of inverter B and inverter C are listed in Table VII.

Two surrogate models of target inverter can be obtained by training from scratch or fine-tuning the existing model of source inverter. Fig. 13 compares the model accuracy under different operational data amount of target inverter, where the solid lines represent the average modeling accuracy and the areas denote the variation of modeling accuracy. The comparison indicates that cross extrapolation form source

TABLE VI
ACCURACY METRICS OF EXPERIMENT C-1 AND C-2

Features	Metrics	Experiment C-1				Experiment C-2			
		RNN	LSTM	NODE	PIML	RNN	LSTM	NODE	PIML
i_a (A)	MAE	0.678	0.429	0.478	**0.196**	1.334	0.356	0.354	**0.267**
	R^2	0.9946	0.9950	0.9976	**0.9995**	0.9951	0.9997	0.9997	**0.9998**
i_b (A)	MAE	1.615	0.586	0.435	**0.163**	2.384	0.185	0.433	**0.163**
	R^2	0.9695	0.9762	0.9976	**0.9997**	0.9781	0.9999	0.9995	**0.9999**
i_c (A)	MAE	1.250	0.460	0.511	**0.140**	2.561	0.369	0.618	**0.154**
	R^2	0.9832	0.9905	0.9964	**0.9998**	0.9732	0.9996	0.9992	**0.9999**
P (W)	MAE	818.6	337.5	192.5	**105.7**	1511.9	134.6	208.6	**118.2**
Q (var)	MAE	295.3	109.9	276.2	**52.1**	384.5	164.5	123.1	**78.0**

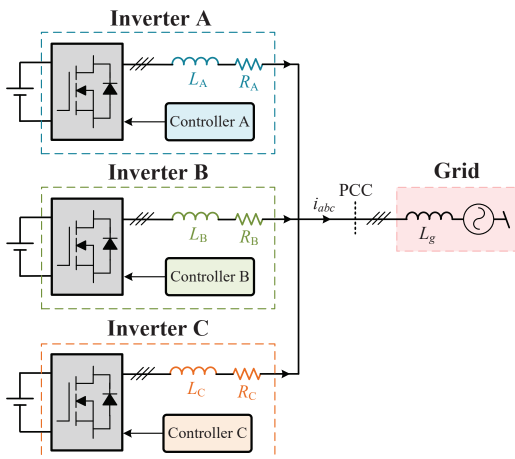

Fig. 12. System configuration of the studied multi-inverter system.

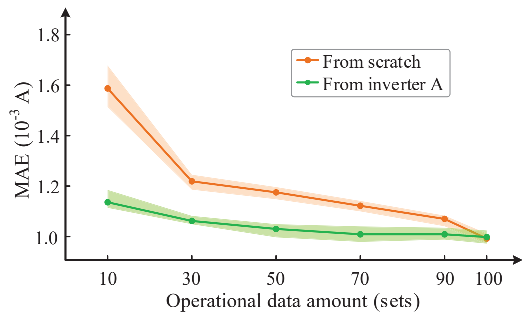

Fig. 13. Transfer learning performance evaluation for the model cross extrapolation from source inverter to target inverter under different operational data amount.

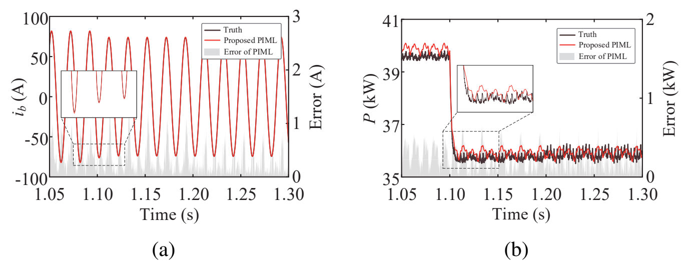

Fig. 14. Measurement and estimation of partial output features in multi-inverter system of experiment D-1.

TABLE VII
PARAMETERS OF TARGET INVERTER

Parameter description	Value
Filter Inductor L	6 mH
Parasitic resistance of filter inductor R_L	0.10 Ω
Proportional parameter of the current controller K_{p_i}	6.5
Integral parameter of the current controller K_{i_i}	20
Proportional parameter of the PLL K_{p_PLL}	8
Integral parameter of the PLL K_{i_PLL}	5000

inverter A can achieve modeling performance comparable to or better than training from scratch method while requiring significantly less data. Moreover, transfer learning based model cross extrapolation consumes much less computational resources, the average time consumption of the two methods is shown in Table VIII. Overall, transfer learning based cross extrapolation has advantages in both computational resources and operational data consumption.

Inverter A in the multi-inverter system as shown in Fig. 12 is the source model trained via 100 sets of operational data, inverter B and inverter C are models extrapolated from inverter A using 50 sets of target operational data for training.

TABLE VIII
AVERAGE TIME CONSUMPTION OF DIFFERENT MODELING METHODS FOR TARGET INVERTER

Method	Cross extrapolation	Traning from scratch
Time	26 min 22 s	37 min 4 s

1) Experiment D-1: Power Instructions Change:

When P_{ref} of inverter A decreases from 14 kW to 10 kW at 1.1 s (maintain Q_{ref} at 2 kvar), Q_{ref} of inverter B increases from 1 kvar to 2 kvar at 1.2 s (maintain P_{ref} at 13 kW) and maintaining P_{ref} of inverter C at 13 kW and Q_{ref} at 2 kvar, the estimation results and scatter plot of partial features are shown in Fig. 14 and Fig. 15, and accuracy metrics are shown in Table IX.

2) Experiment D-2: Short Circuit Fault:

Set P_{ref} to 13 kW and Q_{ref} to 1 kvar for three inverters, and three-phase short circuit fault is set on power grid at 1.1 s, causing the grid voltage to drop to 80% of steady state value, and the fault to be cut off after 0.1 s. The estimation results and scatter plot of partial features of multi-inverter system are shown in Fig. 16 and Fig. 17, and accuracy metrics are shown

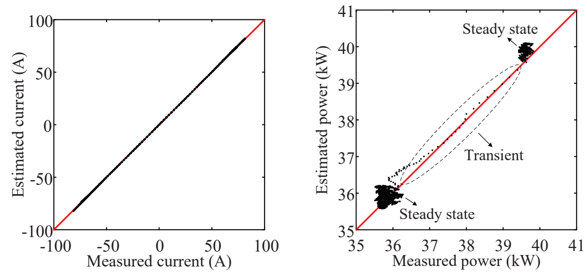

(a) (b)

Fig. 15. Scatter plot of partial output features of experiment D-1. (a) B-phase output current. (b) Active power output.

TABLE IX
ACCURACY METRICS OF EXPERIMENT D-1

Features	i_a (A)		i_b (A)	
Metrics	MAE	R^2	MAE	R^2
Value	0.434	0.9999	0.304	0.9999
Features	i_c (A)		P (W)	Q (var)
Metrics	MAE	R^2	MAE	MAE
Value	0.246	0.9999	216.0	90.9

in Table X.

These results indicate that transfer learning based cross extrapolation of surrogate models is effective and reliable for multi-inverter system. This approach enhances the scalability of surrogate models and improves modeling efficiency, which is of great significance for the simulation analysis of large-scale system.

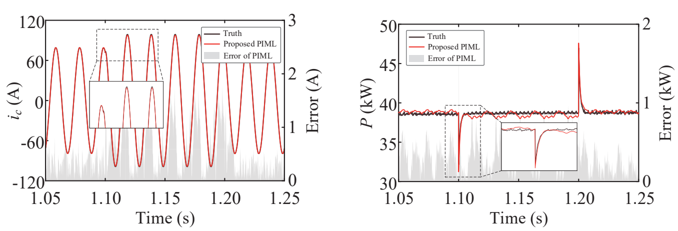

(a) (b)

Fig. 16. Measurement and estimation of partial output features in multi-inverter system of experiment D-2.

TABLE X
ACCURACY METRICS OF EXPERIMENT D-2

Features	i_a (A)		i_b (A)	
Metrics	MAE	R^2	MAE	R^2
Value	0.576	0.9999	0.615	0.9999
Features	i_c (A)		P (W)	Q (var)
Metrics	MAE	R^2	MAE	MAE
Value	0.497	0.9999	304.5	170.2

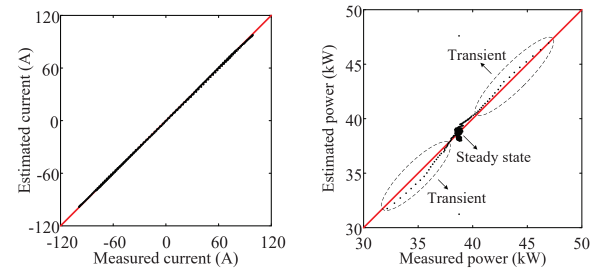

(a) (b)

Fig. 17. Scatter plot of partial output features of experiment D-2. (a) C-phase output current. (b) Active power output.

TABLE XI
COMPUTATIONAL COSTS OF SIMULATING FOR 10 SECONDS

Simulation object	single-inverter	multi-inverter
PIML-based surrogate model	3.2 s	8.5 s
Detailed numerical model	238.9 s	684.5 s

E. Computational Costs and Robustness Analysis of PIML-based Surrogate Model

The proposed inverter surrogate model consists of lightweight neural networks, the surrogate model performs end-to-end inference of system output signals from streaming input signals during simulation, eliminating the need for iterative numerical solving required in conventional simulation approaches. Consequently, system simulations based on the proposed surrogate models achieve significantly faster computational speeds compared to conventional numerical methods. Table XI presents the computational costs required for simulating both single-inverter and multi-inverter systems over a 10 second using different models. The results demonstrate that the proposed modeling method provides notable advantages in accelerating large-scale system simulations.

When applying the proposed method in practical engineering scenarios, the input operational data of the grid-tied inverter surrogate model may contain noise signals. Therefore, the model's robustness under noise is essential. By adding varying levels of white noise signals to the dc-side voltage of the grid-tied inverter surrogate model, we analyzed the variation in the surrogate model's accuracy. The specific results are presented in Table XII. It can be observed that the PIML-based surrogate model maintains high accuracy when the noise intensity is below 20 dB, and the model's accuracy slightly declines when the noise reaches 30 dB. These results demonstrate that the inverter surrogate model generated by the proposed modeling method exhibits strong robustness.

F. Experiment Validation

To further validate the effectiveness of the PIML-based surrogate models, the experimental setup via OPAL-RT system shown in Fig. 18 has been developed, and the parameters of the grid-tied inverters in experiment are listed in Table I and Table VII.

TABLE XII
THE ERROR OF PIML-BASED SURROGATE MODEL UNDER NOISE

Nosie (dB)	0	10	20	30
MAE	0.107	0.108	0.121	0.512
R^2	0.9999	0.9999	0.9999	0.9972

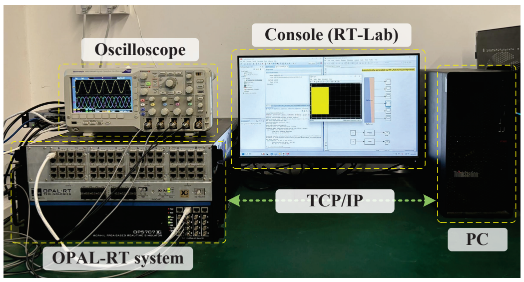

Fig. 18. Experimental setup.

Primary verification focuses on assessing the operational validity of the single PIML-based inverter surrogate model in OPAL-RT system, two cases of different operating scenarios are tested for single inverter (scenario I: P_{ref} is 8 kW, Q_{ref} is 2 kvar; scenario II: P_{ref} changes from 14 kW to 10 kW, and Q_{ref} is 1 kvar). The corresponding experimental results are shown in Fig. 19, where v_a represents the grid voltage (scaling with 0.01) and i_a, i_b and i_c are the output current (scaling with 0.1) of inverter, the scaling operation is due to the output range limitation of the OPAL-RT experimental system.

Construct the multi-inverter system as shown in Fig. 12 in OPAL-RT system using PIML-based surrogate models, two cases of different operating scenarios are tested for multi-inverter system (scenario I: P_{ref} of inverter A is 10 kW, P_{ref} of inverter B and C is 6 kW, Q_{ref} of inverter A, B and C is 1 kvar; scenario II: P_{ref} changes from 6 kW to 12 kW, P_{ref} of inverter B and C is 6 kW, Q_{ref} of inverter A is 2 kvar, Q_{ref} of inverter B and C is 1 kvar). The corresponding experimental results are shown in Fig. 20.

The comprehensive case studies in Section IV prove the simulation effectiveness of the surrogate models generated with the proposed modeling method, which shows the potential of the proposed method in enhancing the simulation of renewable power system.

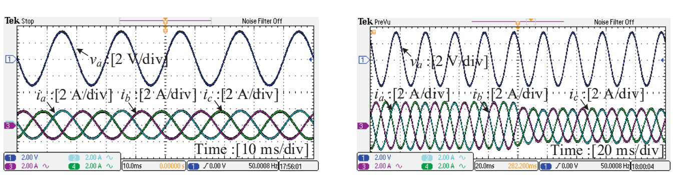

(a) (b)

Fig. 19. Experimental results of single inverter at different operating scenarios. (a) Scenario I: steady state. (b) Scenario II: power instructions change.

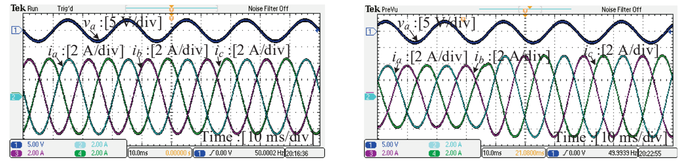

(a) (b)

Fig. 20. Experimental results of multi-inverter system at different operating scenarios. (a) Scenario I: steady state. (b) Scenario II: power instructions change.

V. CONCLUSION

This article proposes a novel modeling approach for black-box grid-tied inverters in renewable power system without access to internal information. The approach is driven by a PINN embedded with DAEs structure and the customized loss function, which can provide the high-precision and physically consistent models for grid-tied inverters. These obtained models are further encapsulated as surrogate models and seamlessly integrated into simulation platform as plug-and-play dynamic components, facilitating accurate and reliable simulation analysis. Furthermore, the application of transfer learning enables cross extrapolation of surrogate models about different inverters, which is well-suited for inverters with scarce operational data, maintaining accuracy while significantly conserving computational resources and operational data consumption. Validations of various case studies demonstrate the effectiveness and superiority of the proposed approach, highlighting its potential in renewable power system simulation analysis. Future work will integrate the proposed surrogate models into actual microgrid with other power electronics devices, leveraging their plug-and-play capability to study microgrid system-level behaviors.

REFERENCES

[1] P. Roy, J. He, T. Zhao, and Y. V. Singh, "Recent advances of wind-solar hybrid renewable energy systems for power generation: A review," *IEEE Open J. Ind. Electron. Soc.,* vol. 3, pp. 81–104, Jan. 2022.

[2] F. Blaabjerg, Y. Yang, K. A. Kim, and J. Rodriguez, "Power electronics technology for large-scale renewable energy generation," *Proc. IEEE,* vol. 111, no. 4, pp. 335–355, Apr. 2023.

[3] Z. Huang, C. Yuan, H. Ge, and T. Hou, "Optimization of substation siting and connection topology in offshore wind farm based on modified firefly algorithm," *IEEE J. Emerg. Sel. Topics Circuits Syst.,* vol. 13, no. 3, pp. 806–816, Sep. 2023.

[4] Y. Gu and T. C. Green, "Power system stability with a high penetration of inverter-based resources," *Proc. IEEE,* vol. 111, no. 7, pp. 832–853, Jun. 2022.

[5] S. Wang, Z. Liu, J. Liu, D. Boroyevich, and R. Burgos, "Small-signal modeling and stability prediction of parallel droop-controlled inverters based on terminal characteristics of individual inverters," *IEEE Trans. Power Electron.,* vol. 35, no. 1, pp. 1045–1063, May. 2019.

[6] S. Subedi, Y. Gui, and Y. Xue, "Applications of data-driven dynamic modeling of power converters in power systems: an overview," *IEEE Trans. Ind. Appl.,* vol. 61, no. 2, pp. 2434–2456, Jan. 2025.

[7] K. Huang, Y. Liu, K. Sun, and F. Qiu, "PI-controlled variable time-step power system simulation using an adaptive order differential transformation method," *IEEE Trans. Power Syst.,* vol. 39, no. 5, pp. 6332–6344, Sep. 2024.

[8] A. Francés, R. Asensi, O. Garcia, R. Prieto, and J. Uceda, "Modeling electronic power converters in smart DC microgrids—An overview," *IEEE Trans. Smart Grid,* vol. 9, no. 6, pp. 6274–6287, Nov. 2018.

[9] L. Qiao, Y. Xue, Y. Gui, W. Du, and F. Wang, "Comparative study of nonlinear black-box modeling for power electronics converters," in *Proc. IEEE Energy Convers. Congr. Expo. (ECCE),* Oct. 2023, pp. 1446–1452.

[10] S. Zhao, F. Blaabjerg, and H. Wang, "An overview of artificial intelligence applications for power electronics," *IEEE Trans. Power Electron.,* vol. 36, no. 4, pp. 4633–4658, Apr. 2021.

[11] E. Kaufhold, S. Grandl, J. Meyer, and P. Schegner, "Feasibility of black-box time domain modeling of single-phase photovoltaic inverters using artificial neural networks," *Energies,* vol. 14, no. 8, p. 2118, Apr. 2021.

[12] G. Rojas-Duenas, J. R. Riba, K. Kahalerras, M. Moreno-Eguilaz, A. Kadechkar, and A. Gomez-Pau, "Black-box modelling of a DC-DC buck converter based on a recurrent neural network," in *Proc. IEEE Int. Conf. Ind. Technol. (ICIT),* Feb. 2020, pp. 456–461.

[13] G. Rojas-Duenas, J. R. Riba, and M. Moreno-Eguilaz, "Black-box modeling of DC-DC converters based on wavelet convolutional neural networks," *IEEE Trans. Instrum. Meas.,* vol. 70, pp. 1–9, Oct. 2021.

[14] P. Qashqai, K. Al-Haddad, and R. Zgheib, "Modeling power electronic converters using a method based on long-short term memory (LSTM) networks," in *Proc. IECON 46th Annu. Conf. IEEE Ind. Electron. Soc.,* Oct. 2020, pp. 4697–4702.

[15] J. Tian, G. Zeng, J. Zhao, X. Zhu, and Z. Zhang, "A data-driven modeling method of virtual synchronous generator based on LSTM neural network," *IEEE Trans. Ind. Inf.,* vol. 20, no. 4, pp. 5428–5439, Apr. 2024.

[16] Q. Shang, F. Xiao, Y. Fan, W. Kang, H. Qin, and R. Wang, "Effinformer: A deep-learning-based data-driven modeling of DC-DC bidirectional converters," *IEEE Trans. Instrum. Meas.,* vol. 72, pp. 1–13, Oct. 2023.

[17] G. E. Karniadakis, I. G. Kevrekidis, L. Lu, P. Perdikaris, S. Wang, and L. Yang, "Physics-informed machine learning," *Nature Rev. Phys.,* vol. 3, no. 6, pp. 422–440, May. 2021.

[18] M. Raissi, P. Perdikaris, and G. E. Karniadakis, "Physics-informed neural networks: A deep learning framework for solving forward and inverse problems involving nonlinear partial differential equations," *J. Comput. Phys.,* vol. 378, pp. 686–707, Feb. 2019.

[19] B. Huang and J. Wang, "Applications of physics-informed neural networks in power systems: A review," *IEEE Trans. Power Syst.,* vol. 38, no. 1, pp. 572–588, Jan. 2023.

[20] S. Zhao, Y. Peng, Y. Zhang, and H. Wang, "Parameter estimation of power electronic converters with physics-informed machine learning," *IEEE Trans. Power Electron.,* vol. 37, no. 10, pp. 11567–11578, Oct. 2022.

[21] H. Ge, Y. Liang, J. Lei, C. Yuan, and Z. Huang, "Neural ODE model of power electronic converters with accelerated computation and high fidelity," *IEEE Trans. Circuits Syst. I Reg. Papers,* vol. 71, no. 12, pp. 6363–6374, Dec. 2024.

[22] X. Li, F. Lin, H. Wang, X. Zhang, H. Ma, C. Wen, and F. Blaabjerg, "Temporal modeling for power converters with physics-in-architecture recurrent neural network," *IEEE Trans. Ind. Electron.,* vol. 71, no. 11, pp. 14111–14123, Mar. 2024.

[23] M. Zhang, P. I. Gómez, Q. Xu, and T. Dragicevic, "Review of online learning for control and diagnostics of power converters and drives: Algorithms, implementations and applications," *Renew. Sustain. Energ. Rev.,* vol. 186, Oct. 2023, Art. no. 113627.

[24] Y. Li, G. Ma, J. Yang, H. Wang, J. Feng, and Y, Ma, "Dynamic equivalent modeling for power converter based on LSTM neural network in wide operating range," *Energy Rep.,* vol. 7, pp 477–484, Apr. 2021.

[25] J. Schmidhuber, "Deep learning in neural networks: An overview.," *Neural Netw.,* vol. 61, pp. 85–117, Jan. 2015.

[26] R. T. Chen, Y. Rubanova, J. Bettencourt, and D. K. Duvenaud, "Neural ordinary differential equations," in *Proc. 32nd Int. Conf. Neural Inf. Process. Syst.,* Dec. 2018, pp. 6572–6583.

[27] C. Moya and G. Lin, "DAE-PINN: a physics-informed neural network model for simulating differential algebraic equations with application to power networks," *Neural Comput. Appl.,* vol. 35, no. 5, pp 3789–3804, Oct. 2022.

[28] P. Hu, W. Yang, Y. Zhu, and H. Liu, "Revealing hidden dynamics from time-series data by ODENet," *J. Comput. Phys.,* vol. 461, Jul. 2022, Art. no. 111203.

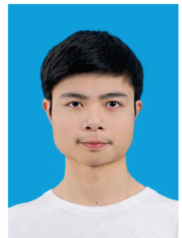

Canjun Yuan received the B.Eng. degree in automation from Wuhan University of Science and Technology, Wuhan, China, in 2022. He received the M.Eng. degree in electronic information at the Shien-Ming Wu School of Intelligent Engineering, South China University of Technology, Guangzhou, China, in 2025.

His research interests include artificial intelligence in power electronics and renewable power system.

Changyue Zou (Senior Member, IEEE) received the B.S. and Ph.D. degrees from the Huazhong University of Science and Technology, Wuhan, China, in electrical engineering in 2010 and 2015, respectively.

He is currently an Electrical Engineer with the Electric Power Research Institute, China Southern Power Grid Co., Ltd., Guangdong. His main research interests include control and design of VSC-HVDC and offshore wind power transmission.

Zhicong Huang (Senior Member, IEEE) received the B.Eng. degree in electrical engineering and automation and the M.Eng. degree in mechanical and electronic engineering from Huazhong University of Science and Technology, Wuhan, China, in 2010 and 2013, respectively, and the Ph.D. degree in power electronics from The Hong Kong Polytechnic University, Hong Kong, China, in 2018.

Since 2020, he has been an Associate Professor with Shien-Ming Wu School of Intelligent Engineering, South China University of Technology, Guangzhou, China. In 2019, he was a Postdoctoral Fellow under the UM Macao Talent Program with the State Key Laboratory of Analog and Mixed-Signal VLSI, Macau, China. His research interests include wireless power transfer, resonant power conversion, large-scale renewable power generation, artificial intelligence for power electronics, and wave energy converters.

Dr. Huang received the Outstanding Reviewer Award for IEEE TRANSACTIONS ON POWER ELECTRONICS in 2024 and 2021, the Star Reviewer Award for IEEE JOURNAL OF EMERGING AND SELECTED TOPICS IN POWER ELECTRONICS in 2024 and 2023, and the Best Reviewer for IEEE JOURNAL ON EMERGING AND SELECTED TOPICS IN CIRCUITS AND SYSTEMS in 2023. He serves as an Associate Editor of IEEE TRANSACTIONS ON CONSUMER ELECTRONICS.